Hindawi
Geofluids
Volume 2021, Article ID 3181697, 18 pages
https://doi.org/10.1155/2021/3181697

Research Article

Mechanical Properties and Damage Behavior of Rock-Coal-Rock Combined Samples under Coupled Static and Dynamic Loads

Jinzheng Bai,[1,2] **Linming Dou**,[1,2] **Piotr Małkowski**,[3] **Jiazhuo Li**,[4] **Kunyou Zhou**,[1,2] **and Yanjiang Chai**[1,2]

[1]*School of Mines, China University of Mining and Technology, Xuzhou 221116, China*
[2]*State Key Laboratory of Coal Resources and Mine Safety, China University of Mining and Technology, Xuzhou 221116, China*
[3]*AGH University of Science and Technology, al. Mickiewicza Av. 30, 30-059 Krakow, Poland*
[4]*State Key Laboratory of Mining Response and Disaster Prevention and Control in Deep Coal Mines, Anhui University of Science and Technology, Huainan 232000, China*

Correspondence should be addressed to Linming Dou; lmdou@126.com

Received 4 June 2021; Accepted 9 August 2021; Published 1 September 2021

Academic Editor: Zhijie Wen

This research is aimed at investigating the influence of the coal height ratio on the mechanical properties and damage behavior of rock-coal-rock combined samples (RCRCS) under coupled static and dynamic loads. For this purpose, a uniaxial cyclic dynamic loading experiment with four different coal height ratios of RCRCS was conducted. Mechanical properties, failure modes, and wave velocity evolution of RCRCS were analyzed; the process of rock burst under coupled static and dynamic loads in rock-coal-rock combined structure was discussed. The following research results are obtained. (1) The peak strength of RCRCS under static and dynamic load decreases with the increasing coal height ratio as an inverse proportional function. (2) The loading and unloading modulus remains consistent for the same levels of dynamic load; the coal height ratio of 40% may be the limit for the stable value of modulus. (3) The increase of the coal height in RCRCS leads to a gradual increase of the energy release rate; the cracks develop preferentially in coal and then extend to rock sample. The distribution of AE events and damage is consistent with the distribution of passive wave velocity. The research results provide important scientific bases for the guidance of early warning of rock burst.

1. Introduction

Rock burst is a dynamic disaster in mining engineering with a sudden and violent release of elastic energy accumulated in coal and rock, which poses a significant risk to mine safety [1–3]. The number of coal mines in China with rock burst disasters has been raised from 32 in 1985 to more than 253 in 2019 [4]. For rock bursts in China, some typical features were observed: (1) Accidents are mostly occurred next to gobs or advancing working face [5, 6]. (2) Coal bodies were broken into powder and rushed out several meters, accompanied by the extensive collapse of the overburden strata; the weak floor suddenly rushed uplifted and caused the entire roadway section to be closed instantly [7]. (3) Accidents are mostly controlled by high static stress caused by mining disturbance, complex geological environment, and dynamic stress caused by fault slipping, hard roof breaking, and large-charge roof blasting [8, 9]. Observations showed that the clamping effect of roof-floor surrounding rock on the coal body becomes more significant as the mining depth increases. Rock burst is not caused by a single rock layer or coal seam but by the structural damage of the roof-coal-floor combined system. Therefore, it is of great significance to investigate the interaction mechanism of static load and dynamic disturbance in the process of rock burst [10–12].

In recent years, certain researchers have conducted valuable laboratory experiment investigations on mechanical behaviors of coal-rock combined samples. Petukhov and Linkov [13] first discussed the postpeak failure properties of two-body combined samples composed of rock and coal.

Table 1: Burst tendency index of the 3-3# coal seam and siltstone from Yutian coal mine.

Coal burst tendency index				
Dynamic failure duration (ms)	Elastic strain energy index	Bursting energy index	Uniaxial compressive strength (MPa)	Burst tendency classification
37.60	3.44	20.79	17.82	Strong
Siltstone burst tendency index				
Elastic modulus (GPa)		Bending energy index		Strong
12.20		169.88		

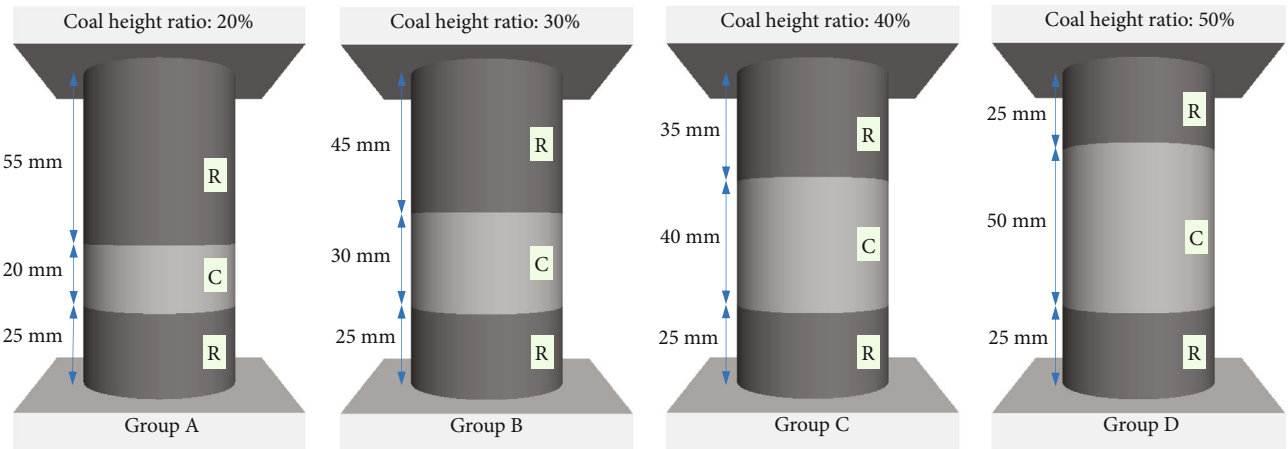

Figure 1: Sketch map of rock-coal-rock combined samples.

Zhao et al. [14] carried out the uniaxial compression test and studied the effect of peak compression strength upon the AE characteristics and P-velocity. Zuo et al. [15] investigated the deformation and failure behavior of rock-coal-rock combined body containing a weak coal interlayer by uniaxial and triaxial tests. Chen et al. [16] analyzed the evolution of internal cracks of coal-rock combined samples based on X-ray computed tomography observations. Zhao et al. [17] established the equivalent homogenous model of coal-rock combined samples and obtained the strength behavior of the combined model composed of different rock mediums and structural plane.

With further in-depth study, researchers are gradually aware that dynamic disturbance functions as an unneglectable external condition among numerous factors that induce rock bursts under deep mining [18, 19]. Zhang et al. [20] studied the energy dissipation characteristics of pure coal samples under multilevel frequency cyclic loading. Gong et al. [21] explored the effect of high loading rate on the mechanical properties of coal-rock combinations. Hu et al. [22] reproduced the cyclic disturbance-induced rock burst in the laboratory using a true triaxial testing system.

However, existing research results mainly focused on the mechanical behavior of coal-rock combined samples under pure static load, while a limited number of studies have been published on the deformation properties and damage behavior of RCRCS under coupled static and dynamic loads. In this study, an experiment of RCRCS with different coal height ratios under coupled static and dynamic loads was conducted. Effects of coal height ratio on mechanical properties, failure mode, and wave velocity evolution of RCRCS are mainly researched in this study. Further, the process of rock burst under coupled static and dynamic loads was discussed, which provides important reference bases for the on-site early warning of rock burst.

2. Methodology

2.1. Sample Preparation. Coal samples used for the experiment were collected from the 3-3# coal seam in Yutian coal mine which is located in Xinjiang Uygur Autonomous Region, China; siltstone samples were collected from the immediate roof of the 3-3# coal seam. According to the Chinese National Standard for Coal Mining Industry, both the coal seam and siltstone layer have an extremely strong burst tendency as shown in Table 1. Numerous researches showed that the coal height ratio has a significant control effect on the mechanical properties of RCRCS [23]. To reflect the clamping effect of roof samples on the coal samples, four sets of samples with different coal heights were prepared for the experiment. Every set had different coal height as shown in Figure 1: group "A"—coal height ratio 20%, group "B"—coal height ratio 30%, group "C"—coal height ratio 30%, and group "D"—coal height ratio 50%. The height of floor siltstone samples was always 25 mm, while the height of roof siltstone samples changed with the coal height.

According to the requirement by the ISRM standard [24], the combined samples were with a diameter of 50 mm and a height of 100 mm. Every part of the RCRCS

Table 2: Physical properties and initial wave velocity of RCRCS.

Coal height ratio (%)	Sample unit	Diameter (mm)	Length (mm)	Mass (g)	Wave velocity (m/s)
	1a1-A1	49.83	100.80	438.6	1828.68
20	1a1-A2	49.96	101.61	421.7	1896.31
	1a1-A3	49.25	100.68	432.8	1912.49
	1a1-B1	49.51	100.04	398.7	1744.27
30	1a1-B2	49.80	101.42	426.8	1738.04
	1a1-B3	49.68	100.47	413.1	1813.16
	1a1-C1	49.51	100.70	422.7	1710.57
40	1a1-C2	49.10	101.50	397.4	1695.36
	1a1-C3	50.04	101.37	438.6	1743.45
	1a1-D1	49.09	101.38	421.7	1566.54
50	1a1-D2	49.29	100.09	403.2	1468.28
	1a1-D3	50.15	100.78	429.3	1347.06

was bonded with super glue; physical properties and initial wave velocity of RCRCS were listed in Table 2.

2.2. Test Device and Measuring System. The tests were carried out in the State Key Laboratory of Coal Resources and Safe Mining of China University of Mining and Technology. The test system is divided into a loading system, an acoustic emission monitoring system, and a high-speed camera system (Figure 2). The 370.50 fatigue-testing machine produced by MTS Corporation in the United States was used to perform multilevel cyclic dynamic load, with a maximum load of 500 kN. The loading system can realize constant amplitude, variable amplitude, and block waveform loading. The PCI-II monitoring system produced by PAC Corporation was applied to capture AE signal features during the test. Eight R15-a sensors were arranged on the surface of the combined sample to be measured through hot melt adhesive to obtain the spatial distribution of AE events. The sampling rate of the system was 2 MHz and the gain of the preamplifier was set as 40 dB. The values of peak definition time (PDT), hit definition time (HDT), and hit lockout time (HLT) were selected as 50 μs, 200 μs, and 300 μs, respectively. The GX-3 high-speed camera system produced by NAC Corporation in Japan was used to capture the deformation and failure characteristics of combined samples in the whole test, which can shoot 2000 frames per second, showing the resolution of 680 × 480 pixels.

2.3. Test Scheme. The dominant frequency band of a waveform signal of a typical rock burst accident in Yutian coal mine was analyzed. On this basis, the frequency of the applied cyclic dynamic load was determined as 5 Hz by combining with the mechanical properties of the fatigue testing. Relevant research results showed that the strain rate of dynamic load in the coal mine is usually within the range of 10^{-3}·s^{-1}~10^{1}·s^{-1} [25], and the strain rate of cyclic dynamic load considered in this paper is about 10^{-2}·s^{-1}, which meet the above requirements. Therefore, the test results can better reflect the actual situation of rock burst due to external dynamic load disturbance.

The stress-controlled was used in the test, and the loading path was divided into four stages as shown in Figure 3, (I) static load stage: the load reached 10 kN at a rate of 300 N/s from the initial state; (II) hold load stage: the static load remains unchanged for 10 s; (III) cyclic dynamic load stage: the oil source drives the indenter to apply a sinusoidal dynamic load to the samples; (IV) hold load stage: the static load remains unchanged for 10 s. The dynamic load frequency was 5 Hz; the upper and lower load limits are 10 kN in each cyclic dynamic load stage, while 100 cycles were repeated. Afterward, the procedure was repeated in the order of I-II-III-IV until the combined sample was irreversibly damaged; the test was ended.

3. Results

3.1. Strain-Stress Curve. As the most important constitutive relationship in material mechanics, the strain-stress curve can reflect the deformation behavior of the material under a given stress state. Figure 4 illustrates the strain-stress curve of RCRCS with different coal height ratios under coupled static and dynamic loads. To facilitate the analysis, the stress behavior of the pure coal and siltstone sample under static load is drawn for comparison. In addition, from reaching the peak strength to completely losing the load-bearing capacity, both RCRCS and the pure coal sample undergo an obvious yielding stage and fail gradually. However, siltstone samples with higher brittleness have a faster fracture rate and a more violent stress reduction process. The coal height ratio has a key influence on the mechanical properties and failure behavior of RCRCS, which will be analyzed in detail.

The peak strength of the RCRCS with different coal heights under coupled static and dynamic loads is shown in Figure 5. In terms of general rules, the peak stress of RCRCS under coupled static and dynamic loads gradually decreases with the increase of coal height, and higher than the coal samples, lower than the siltstone samples, which is consistent with the conclusions obtained by previous scholars. The relationship between coal height and the peak stress of RCRCS can be described by the inverse proportional function as shown in Equation (1).

$$\sigma_c = 20.6 + \frac{0.57}{h_c}, \tag{1}$$

where σ_c and h_c are peak strength and coal height of RCRCS under coupled static and dynamic loads, respectively.

According to the peak strength of the RCRCS, the $\sigma_c \sim h_c$ curve is divided into three stages. In stage I (coal height ratio between 0–only siltstone was tested and 20%), the peak strength decreases sharply from 77.0 MPa to 23.45 MPa. In stage II (coal height ratio between 20% and 50%), the peak strength experiences a slight decrease from 23.45 MPa to 19.54 MPa. In stage III (coal height ratio between 50% and 100%), the peak strength decreases from 19.54 MPa to 14.59 MPa, which can be defined as a proximate stable trend.

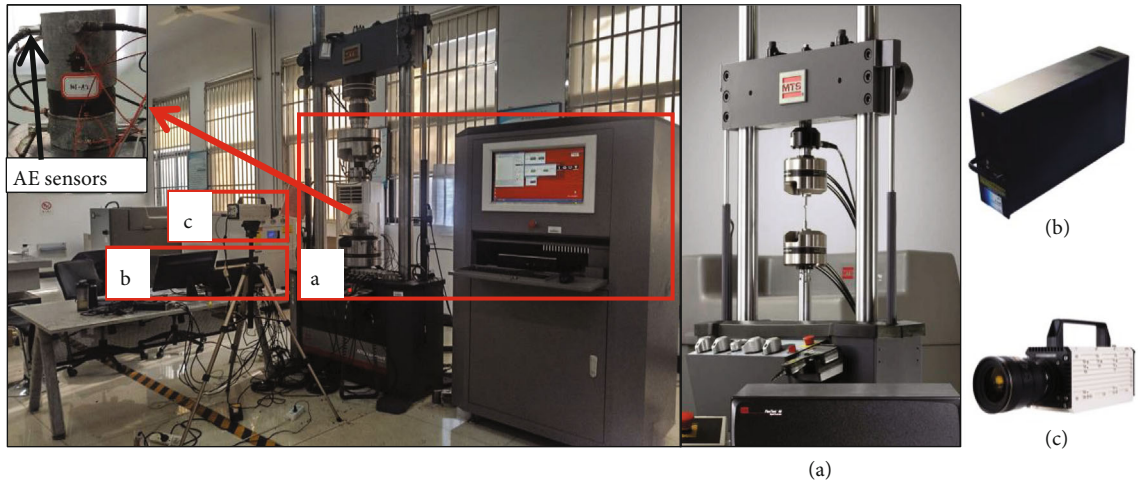

Figure 2: Test device and measuring system. (a) MTS Landmark 370.50; (b) PCI-II AE system; (c) NAG GX-3 high-speed camera.

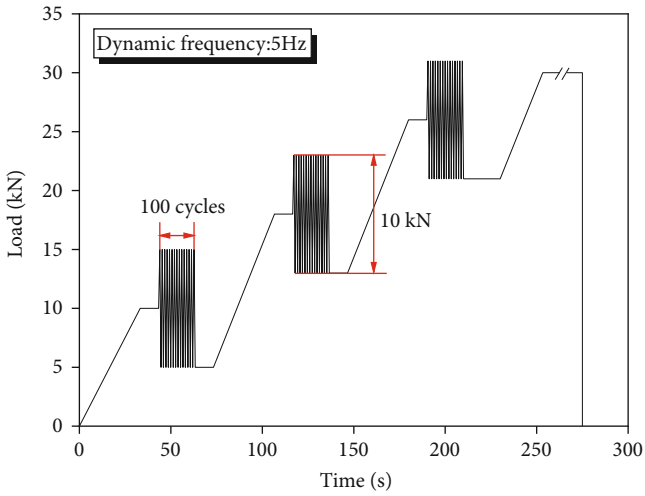

Figure 3: Test loading paths under coupled static and dynamic loads.

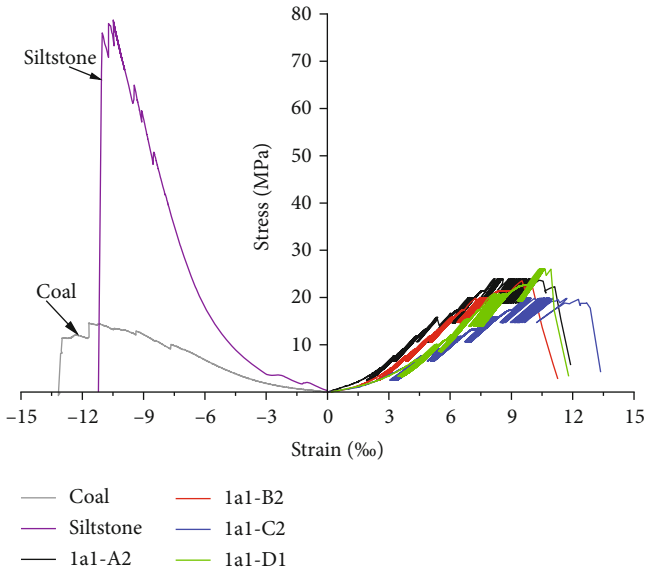

Figure 4: Strain-stress curves of siltstone, coal, and RCRCS.

There, it seems that the critical coal height of 20% and 50% have a key effect on the peak strength of RCRCS.

The static load is applied to the top of the combined samples, while the cyclic dynamic load is applied to the bottom. Regardless of static or dynamic load, once the external load reaches the ultimate bearing strength of the coal sample, the entire RCRCS will lose stability. It can be found that the peak strength under coupled static and dynamic loads is closer to that of the pure coal sample. Therefore, it can be considered that the bearing capacity of RCRCS is closer to the coal sample.

3.2. Elastic Modulus of Cyclic Dynamic Load. The research showed that different loading paths significantly affected the process of connection and coalescence of microfractures. Moreover, the evolution trends of microscopic parameters can be characterized based on various macroscopic parameters, such as elastic modulus and Poisson's ratio [26]. Elastic modulus of coal and rocks reflect their ability to resist deformation under the stress condition, which can be determined under a static load in three different ways [27, 28]. In general, the degree of consolidation between material particles increases with increasing stress. However, the evolution laws of the elastic modulus of RCRCS under cyclic dynamic loading are still unclear. In this paper, the loading elastic modulus E_l and unloading elastic modulus E_u in each hysteresis loop were tested, which also meets the recommendations of ISRM; these two moduli can show the effect of dynamic loads on the RCRCS.

The tangential elastic moduli were calculated using Equation (2) and Equation (3), where σ_A, σ_B, and σ_C are the start, middle, and end stress of each strain-stress loop (hysteresis loop), respectively. As shown in Figure 6, ε_A, ε_B, and ε_C are the start, middle, and end strain of each hysteresis

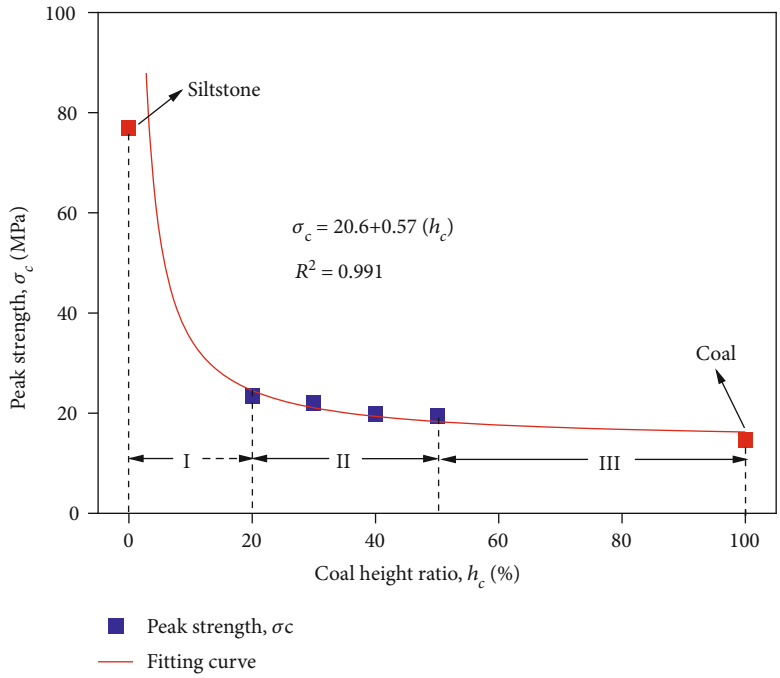

Figure 5: Relation between peak strength of RCRCS and coal height ratio.

loop, respectively. The evolution laws of tangential elastic moduli with the number of cycles at each dynamic stress levels were presented in Figure 7.

$$E_l = \frac{\sigma_B - \sigma_A}{\varepsilon_B - \varepsilon_A}, \tag{2}$$

$$E_u = \frac{\sigma_C - \sigma_B}{\varepsilon_C - \varepsilon_B}. \tag{3}$$

As shown in Figure 7(a), the coal height ratio is 20%. The stress in the compaction stage was relatively low, and the microcracks inside the RCRCS were basically closed. Therefore, the tangential elastic modulus in the first cyclic dynamic load level essentially did not change and maintained a relatively stable value. The average loading modulus value is 3.01 GPa, while the average unloading modulus value is 3.02 GPa in level I. Both were between coal samples (2.08 GPa) and siltstone (12.20 GPa) and closer to that of the coal samples. It was found a slightly increasing trend of the E_l and E_u in the second dynamic load level which was induced by the compaction effect. As the continuously strengthened number of loading cycles, the time of occlusion and reconstruction of microfracture surfaces greatly declined, which inhibited the connection and coalescence of the microfracture surfaces. The average loading modulus value is 3.96 GPa, while the average unloading modulus value is 4.08 GPa in the second dynamic load level. In the third cyclic dynamic load level, the E_l and E_u both showed sharply fluctuated. The average loading modulus value is 4.71 GPa, and the average unloading modulus value is 4.99 GPa. Overall, the elastic modulus in the hysteresis loop increased with an increase in the cyclic dynamic stress level, but the value of the increase was decreased.

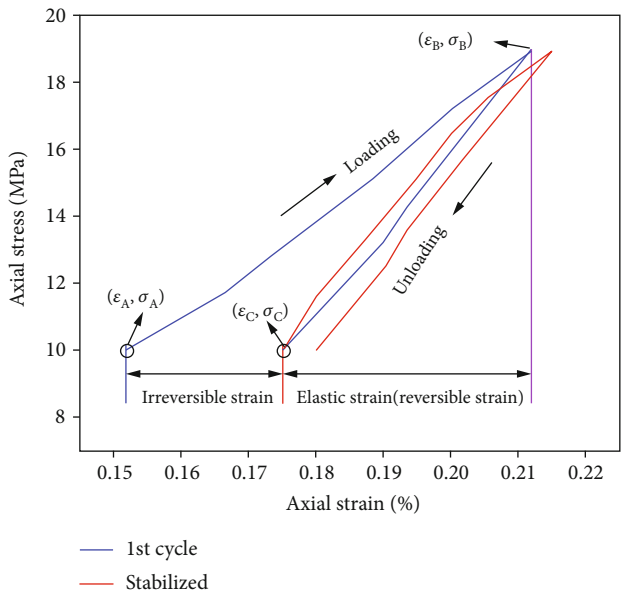

Figure 6: Tangential elastic modulus calculation method in each hysteresis loop.

The failure of 1a1-B2 and 1a1-C2 samples occurred in the fourth cyclic dynamic load stage; a slight decrease and fluctuation trends were observed and caused by damage to the RCRCS owing to cyclic loading, which is representative of the progressive damage of macroscopic parameters. It is worth noting that in the 1a1-D2 sample, the coal height ratio is increased to 50%. A slight decreasing trend of the E_l and E_u in level-I and a remarkable decreasing trend near the failure level can be found. As the proportion of coal height ratio increases, the pores, cracks, and discontinuities inside the

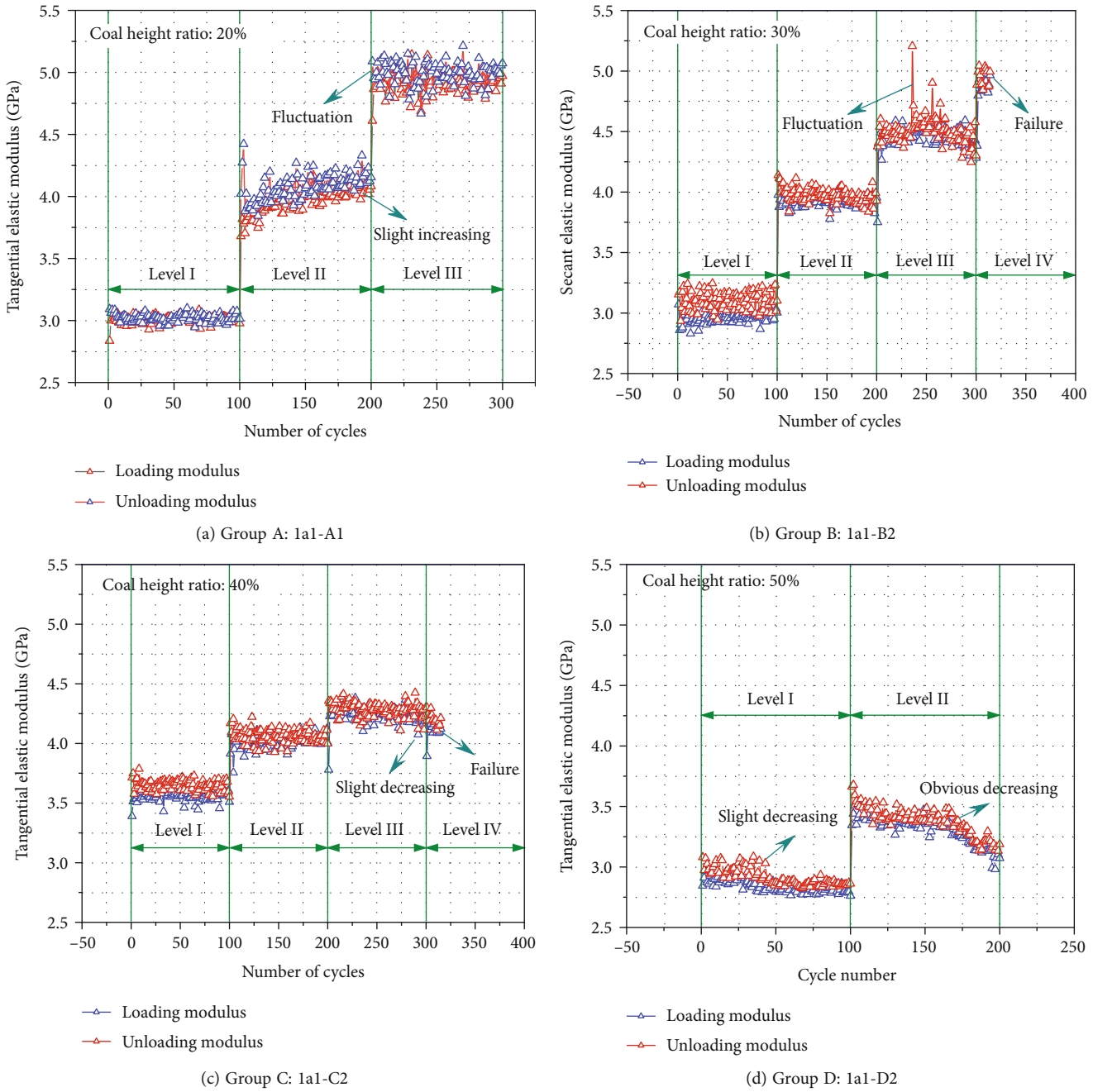

Figure 7: Evolution laws of loading and unloading elastic modulus of RCRCS.

combined structure increase, which further leads to a decrease in the resistance to deformation of the RCRCS. Therefore, the coal height ratio of 40% may be the limit for the stable value of loading and unloading modulus under the dynamic load. For higher coal contribution in the combined samples, it starts cracking under higher loads, and consequent cycles of dynamic loads and modulus values decrease.

In addition, Lei et al. [29] maintained that an increase in the lower stress limit will make the rock harder, while the lower stress limit close to zero will make the rock softer. In this paper, it is also clearly observed that the unloading elastic modulus value is obviously lower than the loading modulus under low-constraint conditions. For the RCRCS which final failure occurred during the dynamic loading level, the two modulus values are basically completely close, indicating that the cyclic dynamic loading caused dense microcrack damage inside the combined sample and reduced the tangential modulus in the hysteresis loop, reflecting the progressive damage characteristics of the RCRCS under the coupled static and dynamic loads.

3.3. The Energy Dissipation. As a quasibrittle material, the RCRCS always exchange energy with the external system under coupled static and dynamic loads. In terms of early warning of rock burst and deeply understanding the fatigue

characteristics of rock, energy dissipation has great significance for damage evaluation. For the RCRCS studied in this paper, part of the energy comes from the heat dissipated by conduction, convection, and radiation, and the other part comes from the energy dissipated by the damage of the material itself. Since the thermal energy of RCRCS general remains unchanged under coupled static and dynamic loads, the energy dissipation trend caused by damage is basically the same as the total energy dissipation. So, the total dissipated energy can be represented by the energy dissipation caused by damage. Energy dissipation of a single hysteresis loop is given by Equation (4), where ε_i, ε_{i+1}, σ_i, and σ_{i+1} are the stress and strain data corresponding to the i and $i+1$ hysteretic loop, respectively. The unit of U_i is J/m^3 which represents the dissipated energy per unit volume between two consecutive data points. The cumulative dissipated energy density U_a is given by Equation (5)–Equation (6), which represents the cumulated dissipated energy from the first cycle to the nth cycle.

$$U_i = \sum_{i=1}^{n} \frac{(\varepsilon_{i+1} - \varepsilon_i)(\sigma_{i+1} - \sigma_i)}{2}, \tag{4}$$

$$U_i = \int_{\min}^{\max} U_i = \oint \sigma d\varepsilon, \tag{5}$$

$$U_a = \sum_{i=1}^{n} U_d. \tag{6}$$

Figure 8 shows the accumulated dissipated energy density of the combined samples with different coal heights at each cyclic dynamic load stage. Obviously, the accumulated dissipated energy increases linearly with the number of cycles within the same stress level, while the rate of increase of the dissipated energy remains unchanged.

The increasing rate of dissipated energy density (slope of the curve) gradually increases with the stress level. The final failure of 1a1-A1 and 1a1-D2 samples were both occurred in the static load stage, while 1a1-B2 and 1a1-C2 were both unstable in the fourth cyclic dynamic load stage. There is an obvious abrupt increment of the accumulated dissipated energy density in the last cycle before the final failure, which indicates that the macroscopic instability of the RCRCS that occurs in the cyclic dynamic loading stage is significantly different from that of the static load stage. In this case, the failure is still brittle, but the accumulated energy is consumed and released rapidly and violently. This is also the essential difference between high stress-dominated and cyclic dynamic load disturbance-dominated rock burst.

The rate of energy dissipation can indicate the mechanical response speed of RCRCS under coupled static and dynamic loads. In this paper, we define a new energy dissipation rate index as: dU_a/dN. Figure 9 plots the quantitative relation between the accumulated energy dissipation density rate of the RCRCS with different coal height ratios and cyclic dynamic stress levels. The relationship between accumulated energy dissipation density rate and the dynamic stress level can be well fitted with an exponential function with high consistency <0.9719~1.00>. Besides, it is clear that with the increase of dynamic stress level, the growth of accumulated energy dissipation density rate increases. This demonstrates that under the higher stress level, the effect of cyclic dynamic load accelerates the growth and penetration speed of microcracks in RCRCS, and the rate of energy release also increases. The combined structure is easier to complete the transformation from a steady state to an unsteady state. In addition, with the increases of coal height ratio in RCRCS, the rate of accumulated energy dissipated density increase, which indicated that as the weaker part of RCRCS, the coal body mainly participates in the response to static and dynamic load, and controls the overall stability.

The total amount of energy dissipation refers to the dissipated energy counting from the first cycle to the last cycle up to failure. Previous studies have shown that the total amount of energy dissipated is constant for specific material such as concrete [30]; it is only related to the stress path and stress level. However, this experiment shows another form of the energy dissipation of RCRCS. Figure 10 shows that the total energy dissipation corresponding to different cycles of dynamic times is quite different, indicating that the total dissipated energy could not be a material constant, but a variable related to the total number of cyclic load cycles.

3.4. Spatial Distribution of AE Events and Failure Mode. The AE source location has been widely used to detect the origin and propagation of cracks in various materials, such as concrete [31], rock [32], rock-like material [33], coal [34], and metal [35]. It can realize the continuous visualization of the spatio-temporal evolution law of material damages in the whole loading process. As shown in Figure 11(a), AE event energy (unit: aJ) can be divided into seven grades.

To reflect the internal fracture propagation and damage development of the RCRCS under coupled static and dynamic loads, the load process is sequentially decomposed into the "static + hold load" stage and the "dynamic + hold load" stage. The failure characteristics of the RCRCS under instantaneous dynamic failure are analyzed by capturing the images of the combinations before failure with the high-speed camera. Limited by the article length, to show the influence of different coal height ratios on the failure modes of the combined samples, the biggest (50%) and smallest (20%) coal height ratios in each group are selected to perform the analysis.

The first analysis considers the 1a1-A1 sample of group "A" with a coal height ratio of 20%. Figure 12(a) indicates that the low-energy AE events are initiated in the middle of the coal body of the RCRCS during the initial static load stage, which is mainly due to the closure of primary cracks and pore. The cyclic dynamic load under low stress levels has no obvious effect on the microfracture of RCRCS. With the increase of stress level, the AE events with large energy evolve from coal sample to the roof siltstone. In the second "dynamic + hold load" stage, the growth of AE events is the most obvious, especially the AE events in the roof rock samples began to gather significantly. In the next "static + hold" stage, the development of microfractures in the coal body is almost full, while there are still only a few low-

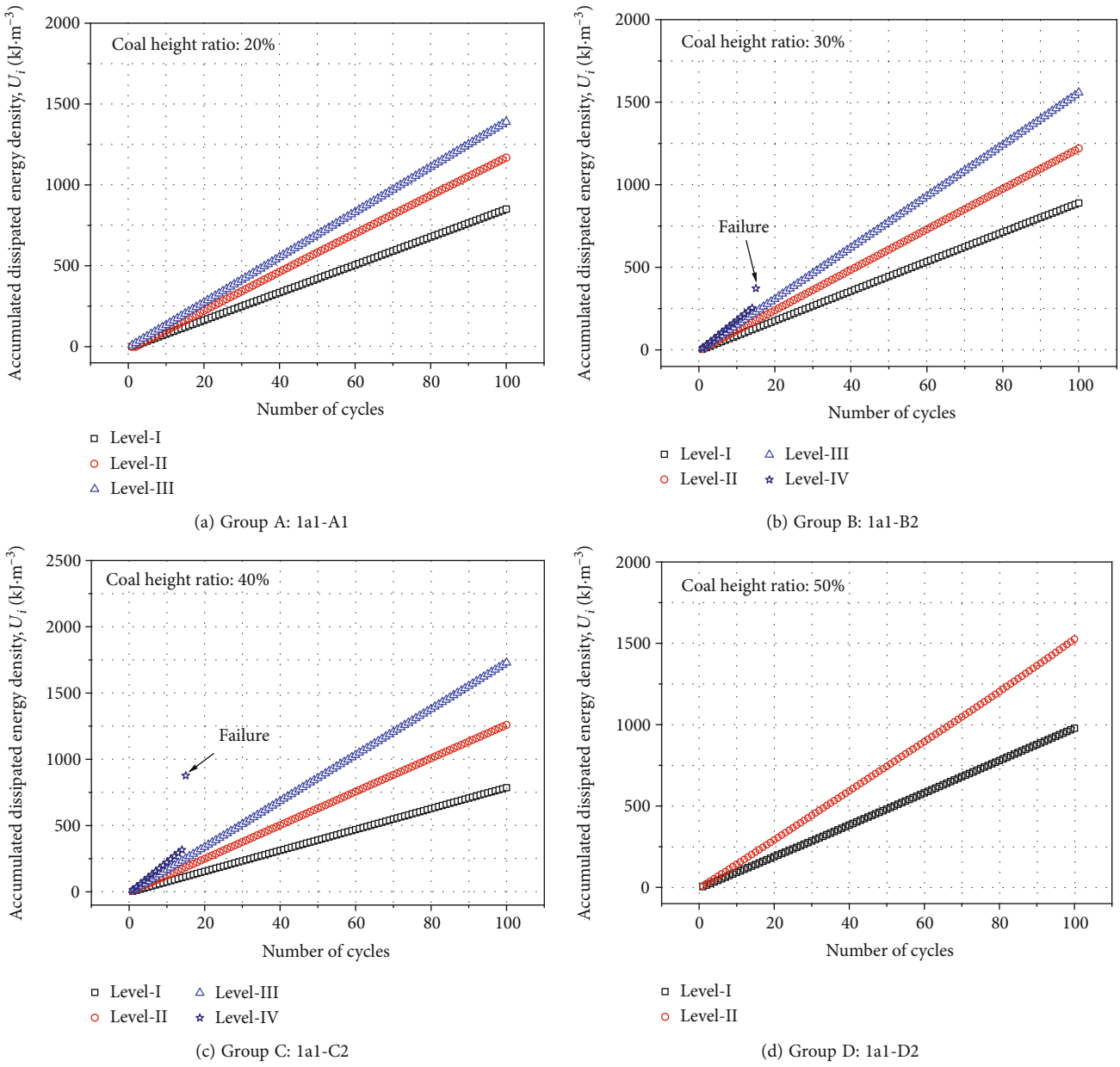

Figure 8: Accumulated dissipated energy density of RCRCS.

energy AE events in the floor rock samples. Until the last "dynamic + hold" load stage, the distribution of AE events in the floor rock sample has been extended to the top end, and the RCRCS structure is close to critical instability. The AE events in the roof rock sample are distributed in a "cone" shape, and the position of its generatrix is the contour where splitting failure occurs, which well corresponds to area A in 1a1-A1 as shown in Figure 12(b). According to the failure process, the coal sample is the first to spray particles, while there is no obvious deformation of the roof and floor siltstone samples. Subsequently, the coal sample showed a visible horizontal volume expansion; the side of the roof rock sample appeared longitudinal splitting failure. A strong impact tendency occurred accompanied by the coal pulver and mass ejection violently.

The second analysis considers the 1a1-D2 sample of group "D" with a coal height ratio of 50%. Figure 13(a) indicates that the AE events are distributed both in the roof, coal, and floor samples in the initial load stress, especially in the interface between the coal and rock samples above and below. The cyclic dynamic load under initial stress levels caused RCRCS to produce a series of low-energy AE energy, different from group "A"; the top and bottom siltstone samples significantly participate in the mechanical response to static and dynamic loads at this time. Subsequent cyclic dynamic load causes the microfractures in the coal body to continue to develop until it reaches a near-destructive state. This indicates that the damage evolution in the RCRCS is not homogenous at the beginning; top and bottom rock parts experience more damage characterized more and

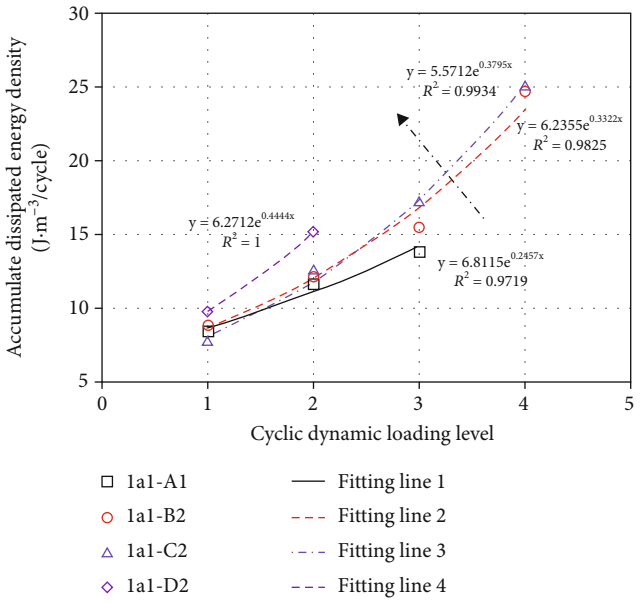

Figure 9: Relation of accumulated energy dissipation density and cyclic dynamic loading level.

stronger AE events. Figure 13(b) documents that the left part of the coal sample burst first out at failure (area B), then the roof siltstone sample showed complete longitudinal splitting failure.

In summary, the damage evolution of RCRCS under coupled static and dynamic loads can be described as follows: (1) When the coal height ratio is small, the damage first initiates in the coal sample, then more and more cracks appear in the roof sample. Finally, the RCRCS was completely destabilized until the macroscopic cracks developed to the top of the roof siltstone sample. (2) When the coal height is large, the damage is distributed both in the roof, floor siltstone and coal samples. The final failure is characterized by the burst failure of the coal sample and the split failure of the siltstone sample, which is consistent with the composite failure pattern of roof-coal-floor described above.

3.5. Distribution of Passive Wave Velocity. Passive velocity tomography is based on the seismic wave velocity of media equaling the result of dividing the length of ray paths by the propagation time of seismic waves from the seismic source to a receiver. In recent years, passive velocity tomography has been extensively used to predict the rock burst hazard in the field [36, 37]. In this part, the wave velocity field is inverted based on the internal wave velocity obtained from the AE source events. Same as the chapter of the spatial distribution of AE events and failure mode, we take 1a1-A1 and 1a1-D2 samples as examples for illustration.

According to the theory of passive velocity tomography, the P-wave velocity variations are linked to the changes of stress. Therefore, the high-velocity zones in tomograms are representing the high-stress zones. In addition, the wave velocity propagation is also related to the physical and mechanical properties of rock and structural properties of the rock mass.

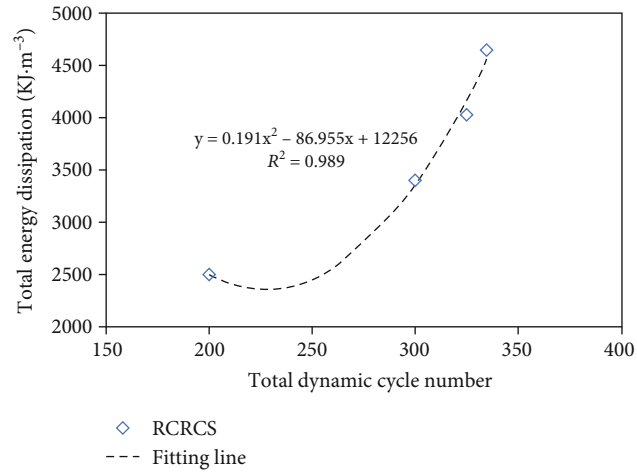

Figure 10: Relation of total amount of energy dissipation and total dynamic cyclic number.

Figure 14(a) indicates that the high-velocity area is mainly concentrated in the middle of the coal and roof siltstone parts in the initial stress level of the 1a1-A1 combined sample, but its concentration is limited. Subsequent cyclic dynamic loads lead to a more concentrated area of wave velocity anomaly, and the degree of concentration is getting higher. Due to the abundant cracks generated inside the RCRCS near the final failure, the strength of the combined structure is reduced and entered a yielding state; the range of high-velocity area is reduced.

Figure 14(b) indicates that the high-velocity area is mainly concentrated in the coal parts of the 1a1-D2 combined sample, while the low-velocity area is scattered around the RCRCS. Due to the high coal body height, it has become the main area that mainly participates in the destruction, and it is also the concentrated area of the high wave velocity abnormal area. The elastic core region is the energy storage region of the RCRCS, which provides the driving force of impact failure in the final failure. The wave velocity distribution is well consistent with the spatial distribution of AE events and failure mode.

4. Discussion

The theoretical model as shown in Figure 15 is established on the basis of the above laboratory experiment results, to deepen the understanding of the impact mechanism of coal-rock mass under coupled static and dynamic loads.

Thanks to the study, it is possible to show the mechanism of rock burst under coupled static and dynamic stresses. Figure 15 plots the energy transfer in the roof-coal-floor systems during the coal burst process under coupled static and dynamic loading. The stress behavior of the surrounding rock is displayed on the left-hand side; the stiffness and strength are both higher than coal. The stress behavior of coal is displayed on the right-hand side, and coal is assumed to be a softening material with nonlinear behavior. In the roof-coal-floor combined system, if the strain $\Delta\varepsilon_2$ is produced in the coal sample under the static load, the corresponding strain will be produced synchronously in the

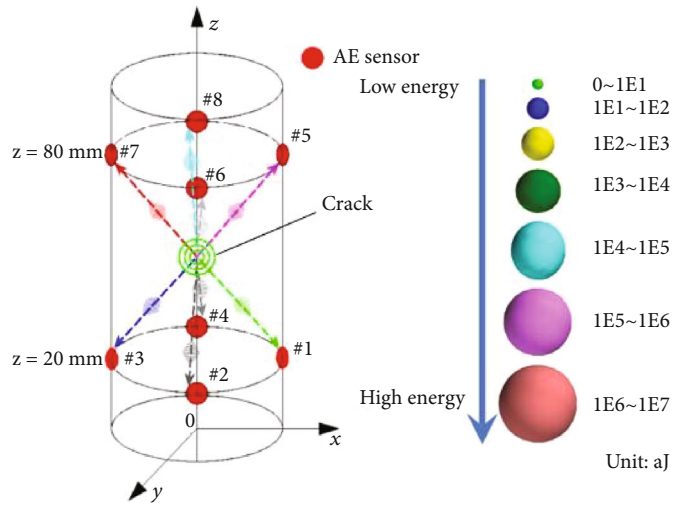

Figure 11: Layout of AE monitoring system and categorization of AE events.

surrounding rock (roof and floor) $\Delta\varepsilon_1$; the relationship between $\Delta\varepsilon_1$ and $\Delta\varepsilon_2$ can be expressed as

$$\Delta\varepsilon_1 = \frac{k_2}{k_1}\Delta\varepsilon_2, \tag{7}$$

where k_1 is the stiffness of surrounding rock and k_2 is the stiffness of coal. Therefore, the total strain of the roof-coal-floor system can be written as

$$\Delta\varepsilon = \Delta\varepsilon_1 + \Delta\varepsilon_2 = \frac{k_1 + k_2}{k_1}\Delta\varepsilon_2. \tag{8}$$

Therefore, the ratio of coal strain to total strain can be written as

$$\frac{\Delta\varepsilon_2}{\Delta\varepsilon} = \frac{1}{1 + (k_2/k_1)}. \tag{9}$$

From Equation (9), if we just consider static load, the process from stability to the instability of coal can be divided into four stages:

(1) Stage AB: both k_1 and k_2 are larger than zero; the coal and surrounding rock are both in the elastic energy storage stage

(2) Stage BD: the coal first enters the inelastic deformation stage. k_1 is still larger than zero, while k_2 gradually decreased to zero at the peak point D. At this time, the coal begins to transform the elastic energy stored into plastic deformation, and the surrounding rock is still in the elastic energy storage stage

(3) Stage DS: the carrying capacity of the coal body gradually loses, and k_2 turns into a negative value. During this process, the roof-coal-floor combined system may undergo an unstable process, when $k_1 + k_2 = 0$, $\Delta\varepsilon_2/\Delta\varepsilon \longrightarrow \infty$. The strain of the roof-coal-floor system expands rapidly in an instant, and the energy accumulated in the coal sample and surrounding rock is released together, which will trigger the overall failure, corresponding to the occurrence of rock burst

(4) Stage SE: the instability of the coal body slows down gradually; the roof-coal-floor system reaches the next stable energetic state, which corresponds to the calm period after the occurrence of the rock burst

When the roof-coal-floor system is subjected to the superposition of external static and dynamic loading stress (σ_s and σ_d), which can be equivalent to a condition that the stiffness of the surrounding rock decreases from k_1 to k_1'. In this context, there are two different situations: (1) disturbance dynamic stress: when the cyclic dynamic load is applied under a low-stress level, it is easier to cause the expansion of microcracks inside the RCRCS, accompanied by small fluctuations in the stress value and a series of AE events, but it will not induce impact instability. (2) Impact-derived dynamic stress: when the cyclic dynamic load is applied near the instability, the stress is more likely to evolve along a path in the 1-2-4 direction, rather than the 1-3-D-4. The additional input energy will be larger, and the coal failure process will be more violent. Therefore, the equivalent energy decrease of the stiffness of the surrounding rock will be more remarkable.

5. Conclusions

The mechanical properties and damage behavior mechanisms of RCRCS under coupled static and dynamic loads were investigated in terms of strain-stress curve, loading and unloading modulus, AE events distribution and failure modes, and wave velocity field. Compared with the failure laws of single coal or rock materials, the prediction of the failure of rock-coal-rock is more complex and difficult. After the investigations, the results can be concluded as follows:

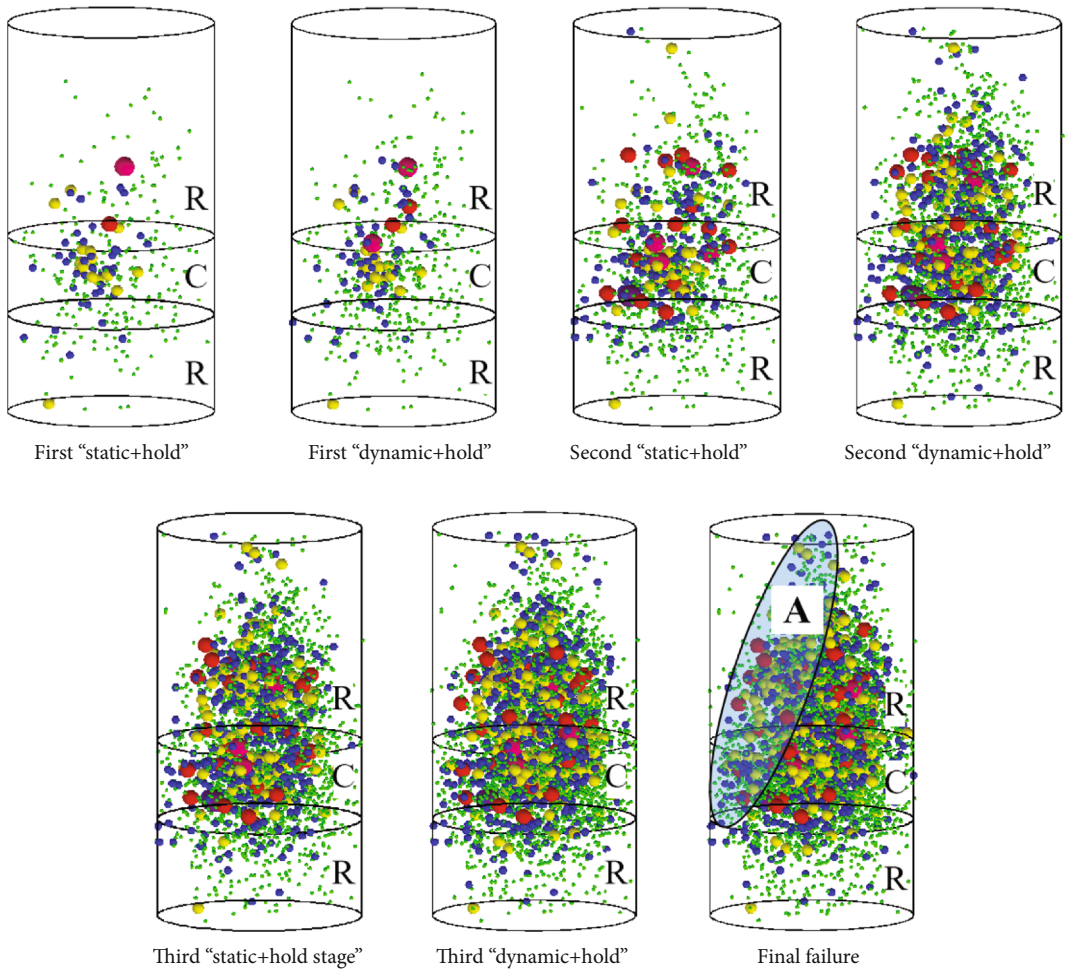

(a)

Figure 12: Continued.

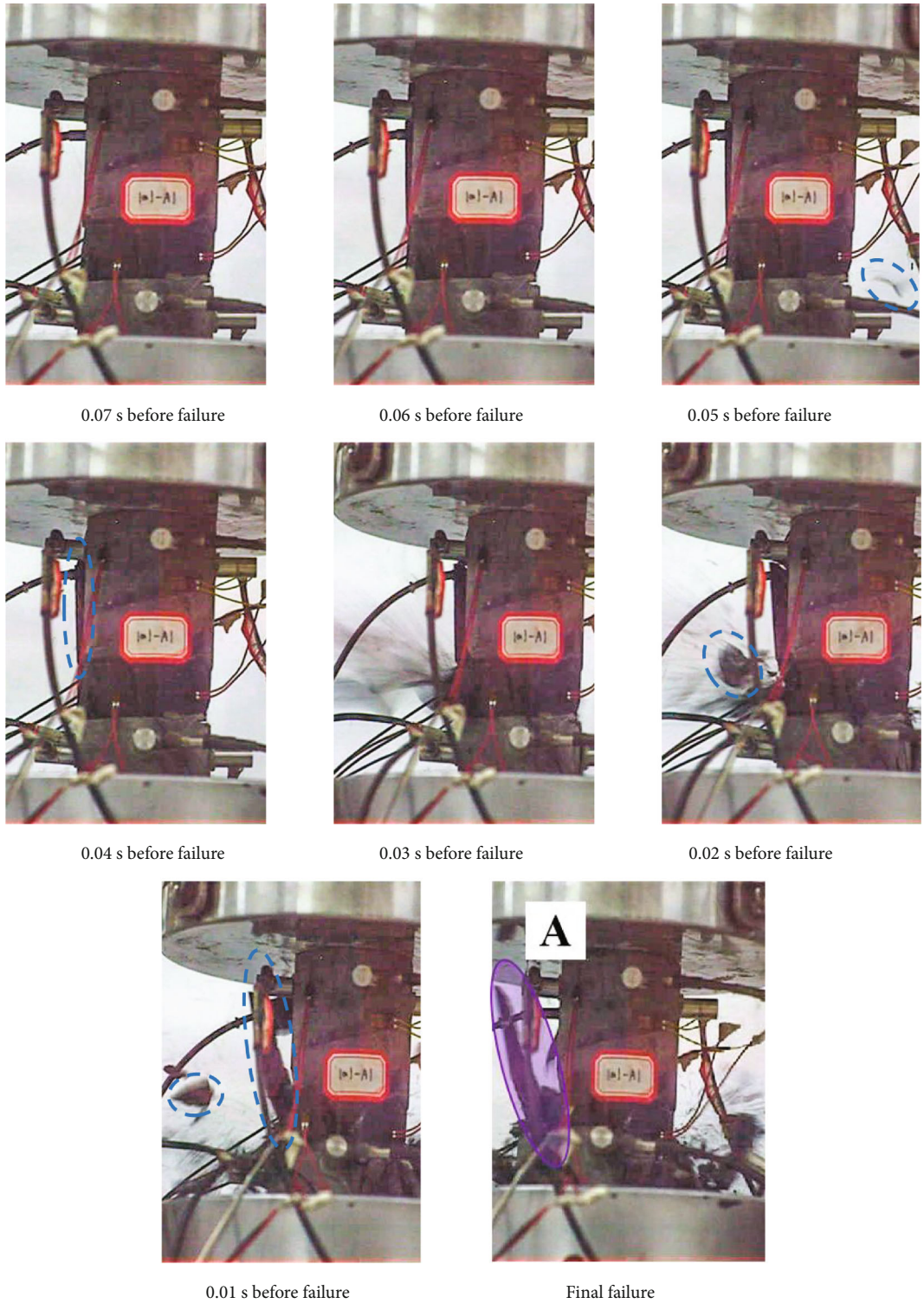

(b)

Figure 12: (a) Spatial distribution of AE events for each stress level of the 1a1-A1 specimen. (b) Failure process of 1a1-A1 specimen captured by high-speed camera.

(1) The peak strength of the RCRCS under coupled static and dynamic loads is strongly affected by the coal height. The coal height versus the peak strength curve is divided into three stages, namely, intensive decline stage (0~20%), moderate decrease stage (20~50%), and stable stage (50~100%)

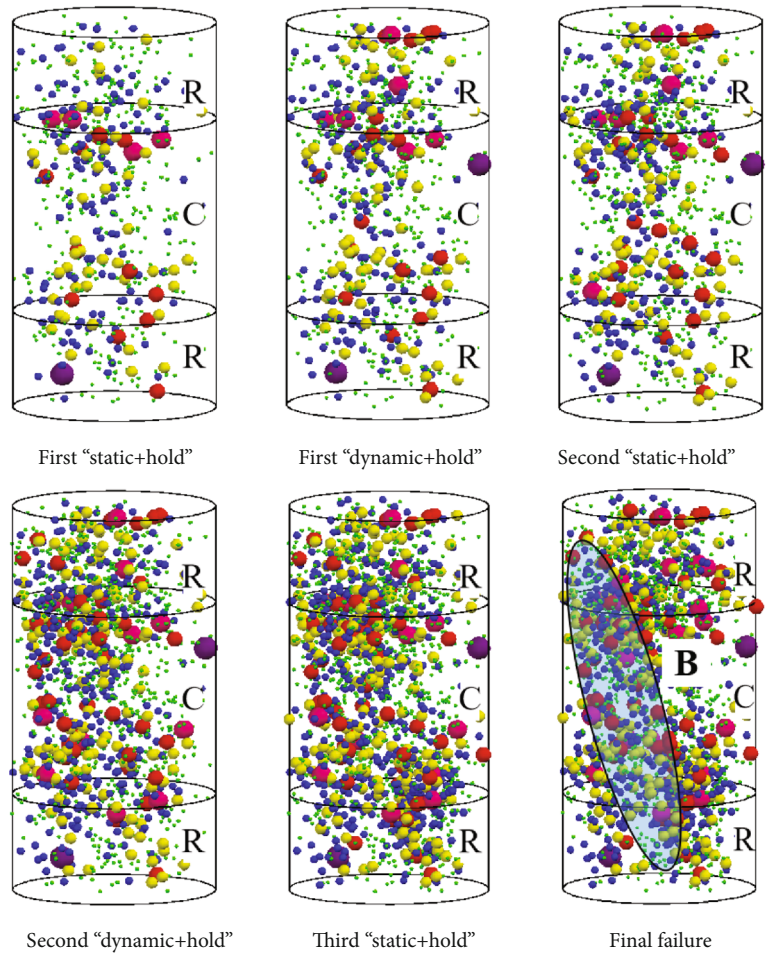

(a)

Figure 13: Continued.

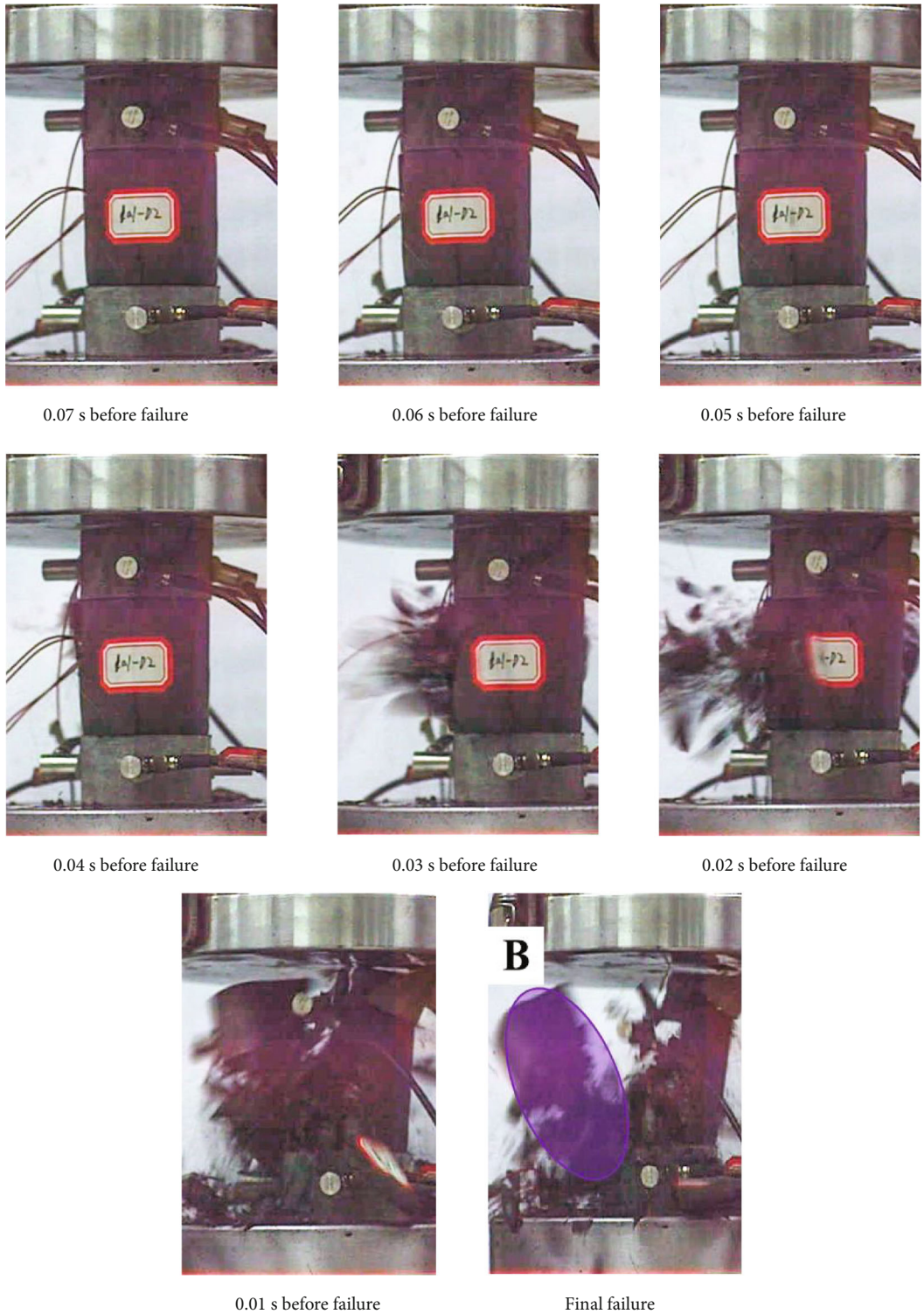

(b)

Figure 13: (a) Spatial distribution of AE events for each stress level of the 1a1-D2 specimen. (b) Failure process of 1a1-D2 specimen captured by high-speed camera.

(2) The loading and unloading modulus remain basically consistent for the same levels of dynamic load, while there is a slight decrease at high-stress levels. The coal height ratio of 40% may be the limit for the stable value of modulus values. For higher coal contribution in the combined samples, it starts cracking under higher loads, and consequent cycles of dynamic loads and modulus values decrease.

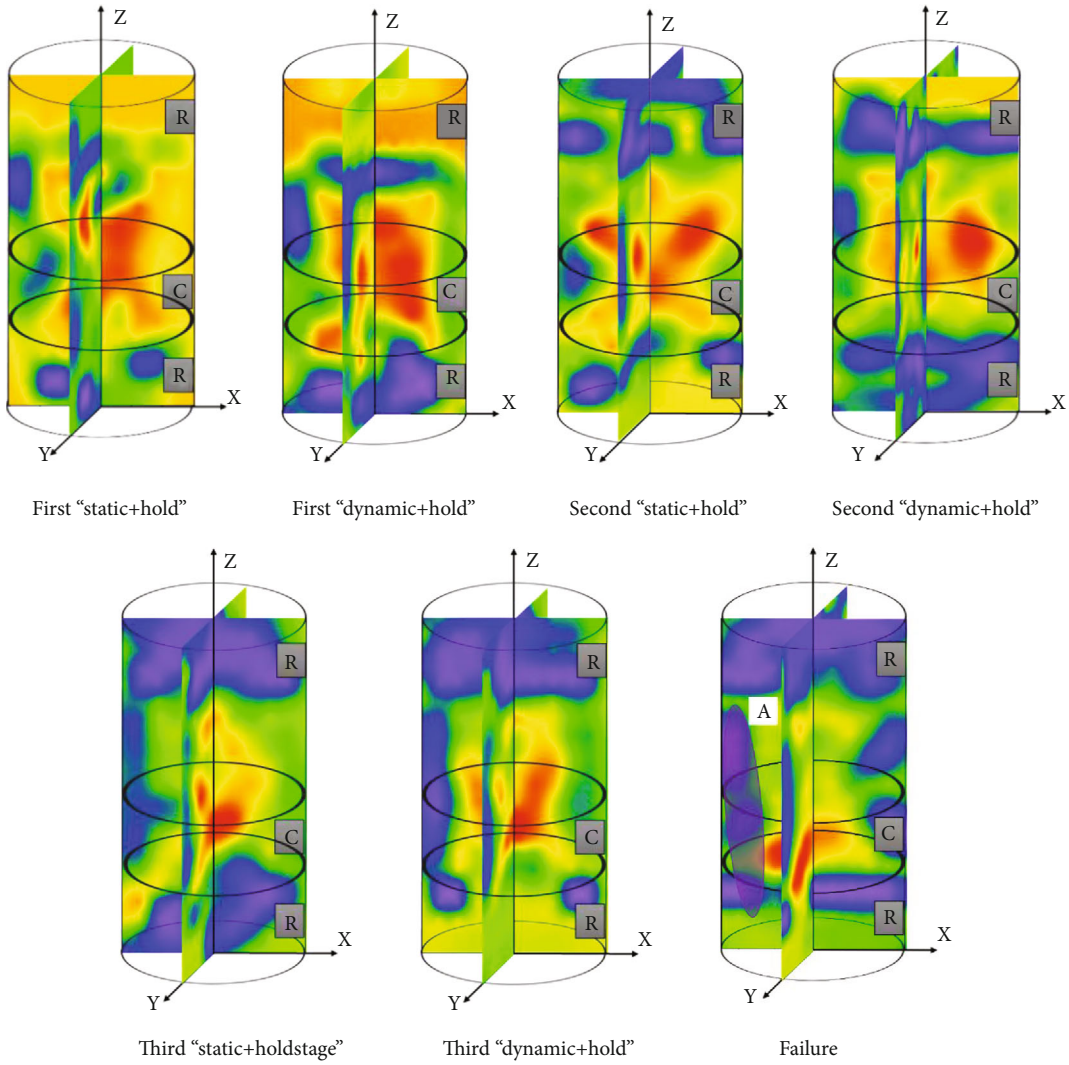

(a) 1a1-A1

Figure 14: Continued.

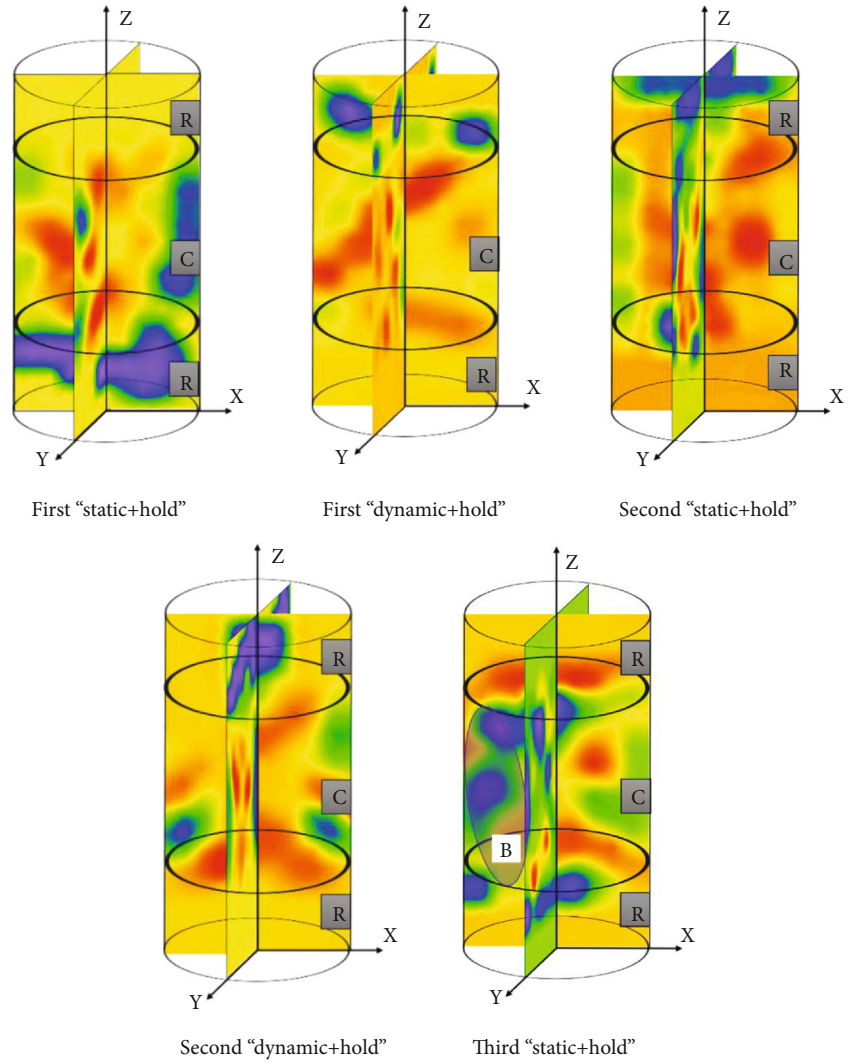

(b) 1a1-D2

Figure 14: Acoustic wave velocity distribution.

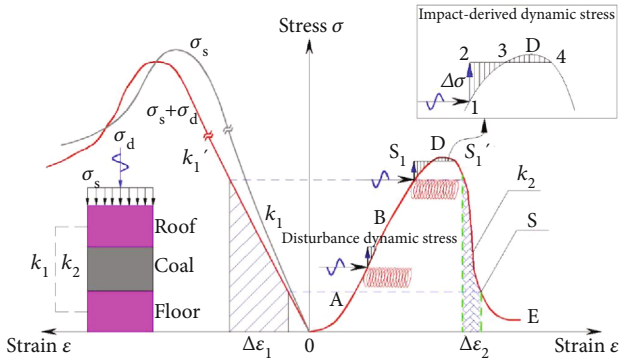

Figure 15: Energy transfer in roof-coal-floor system during the coal burst process under coupled static and dynamic loading.

Moreover, the loading and unloading modulus increase with the stress level

(3) When the coal height ratio is 20%, the damage first initiates in the coal sample, then more and more cracks appear in the roof sample. Otherwise, it will be manifested as the combined damage of the ejection damage of the coal body and the splitting of the roof and floor rocks. The results are consistent with the distribution of passive wave velocity

(4) The physical model of RCRCS tested under coupled static and dynamic stresses explains very well the mechanism of rock burst, which takes place in underground mining

Data Availability

The data used to support the findings of this study are available from the corresponding author upon request.

Conflicts of Interest

The authors declare no conflict of interest.

Acknowledgments

The authors are grateful for the financial support from the National Natural Science Foundation of China (Grant nos. 51874292 and 51804303) and Postgraduate Research & Practice Innovation Program of Jiangsu Province (KYCX21_2342).

References

[1] P. K. Kaiser and M. Cai, "Design of rock support system under rockburst condition," *Journal of Rock Mechanics and Geotechnical Engineering*, vol. 4, no. 3, pp. 215–227, 2012.

[2] W. D. Ortlepp and T. R. Stacey, "Rockburst mechanisms in tunnels and shafts," *Tunnelling and Underground Space Technology*, vol. 9, no. 1, pp. 59–65, 1994.

[3] M. Cai, "Principles of rock support in burst-prone ground," *Tunnelling and Underground Space Technology*, vol. 36, pp. 46–56, 2013.

[4] J. R. Cao, L. M. Dou, G. A. Zhu, J. He, S. Wang, and K. Zhou, "Mechanisms of rock burst in horizontal section mining of a steeply inclined extra-thick coal seam and prevention technology," *Energies*, vol. 13, no. 22, p. 6043, 2020.

[5] Y. D. Jiang, Y. X. Zhao, H. W. Wang, and J. Zhu, "A review of mechanism and prevention technologies of coal bumps in China," *Journal of Rock Mechanics and Geotechnical Engineering*, vol. 9, no. 1, pp. 180–194, 2017.

[6] T. Li, M. F. Cai, and M. Cai, "A review of mining-induced seismicity in China," *International Journal of Rock Mechanics and Mining Sciences*, vol. 44, no. 8, pp. 1149–1171, 2007.

[7] Z. J. Wen, X. Wang, Y. L. Tan, H. L. Zhang, W. P. Huang, and Q. H. Li, "A study of rockburst hazard evaluation method in coal mine," *Shock and Vibration*, vol. 2016, Article ID 8740868, 9 pages, 2016.

[8] W. Cai, X. Q. Bai, G. Si, W. Z. Cao, S. Gong, and L. Dou, "A monitoring investigation into rock burst mechanism based on the coupled theory of static and dynamic stresses," *Rock Mechanics and Rock Engineering*, vol. 53, no. 12, pp. 5451–5471, 2020.

[9] Q. Ma, Y. L. Tan, X. S. Liu, Q. H. Gu, and X. B. Li, "Effect of coal thicknesses on energy evolution characteristics of roof rock-coal-floor rock sandwich composite structure and its damage constitutive," *Composites Part B: Engineering*, vol. 198, article 108086, 2020.

[10] M. C. He, F. Q. Ren, and D. Q. Liu, "Rockburst mechanism research and its control," *International Journal of Mining Science & Technology*, vol. 28, no. 5, pp. 829–837, 2018.

[11] W. C. Zhu, Z. H. Li, L. Zhu, and C. A. Tang, "Numerical simulation on rockburst of underground opening triggered by dynamic disturbance," *Tunnelling and Underground Space Technology*, vol. 25, no. 5, pp. 587–599, 2010.

[12] X. S. Liu, Y. L. Tan, J. G. Ning, Y. W. Lu, and Q. F. Gu, "Mechanical properties and damage constitutive model of coal in coal-rock combined body," *International Journal of Rock Mechanics and Mining Sciences*, vol. 110, pp. 140–150, 2018.

[13] I. M. Petukhov and A. M. Linkov, "The theory of post-failure deformations and the problem of stability in rock mechanics," *International Journal of Rock Mechanics and Mining Sciences & Geomechanics Abstracts*, vol. 16, no. 2, pp. 57–76, 1979.

[14] T. B. Zhao, X. B. Gu, W. Y. Guo et al., "Influence of rock strength on the mechanical behavior and P-velocity evolution of coal-rock combination specimen," *Journal of Materials Research and Technology*, vol. 12, no. 1, pp. 1113–1124, 2021.

[15] J. P. Zuo, Z. Wang, H. Zhou, J. Pei, and J. Liu, "Failure behavior of a rock-coal-rock combined body with a weak coal interlayer," *International Journal of Mining Science & Technology*, vol. 23, no. 6, pp. 907–912, 2013.

[16] Y. L. Chen, J. P. Zuo, D. Liu, and Z. Wang, "Deformation failure characteristics of coal–rock combined body under uniaxial compression: experimental and numerical investigations," *Bulletin of Engineering Geology and the Environment*, vol. 78, no. 5, pp. 3449–3464, 2019.

[17] Z. H. Zhao, W. M. Wang, L. H. Wang, and C. Q. Dai, "Compression–shear strength criterion of coal–rock combination model considering interface effect," *Tunnelling and Underground Space Technology*, vol. 47, pp. 193–199, 2015.

[18] J. Li, J. Zhao, S. Y. Gong et al., "Mechanical anisotropy of coal under coupled biaxial static and dynamic loads," *International Journal of Rock Mechanics and Mining Sciences*, vol. 143, no. 3, article 104807, 2021.

[19] F. Q. Gong, J. Y. Yan, X. B. Li, and S. Luo, "A peak-strength strain energy storage index for rock burst proneness of rock materials," *International Journal of Rock Mechanics and Mining Sciences*, vol. 117, pp. 76–89, 2019.

[20] M. Zhang, L. M. Dou, H. Konietzky, Z. Song, and S. Huang, "Cyclic fatigue characteristics of strong burst-prone coal: experimental insights from energy dissipation, hysteresis and micro-seismicity," *International Journal of Fatigue*, vol. 133, article 105429, 2020.

[21] F. Q. Gong, H. Ye, and Y. Luo, "The effect of high loading rate on the behaviour and mechanical properties of coal-rock combined body," *Shock and Vibration*, vol. 2018, Article ID 4374530, 9 pages, 2018.

[22] L. H. Hu, Y. C. Li, X. Liang, C. A. Tang, and L. B. Yan, "Rock damage and energy balance of strainbursts induced by low frequency seismic disturbance at high static stress," *Rock Mechanics and Rock Engineering*, vol. 53, no. 11, pp. 4857–4872, 2020.

[23] H. W. Zhang, Z. J. Wan, Y. Zhang, and D. Wu, "Mechanical properties and failure behavior of composite samples," *Advances in Materials Science and Engineering*, vol. 2018, Article ID 2545127, 16 pages, 2018.

[24] C. E. Fairhurst and J. A. Hudson, "Draft ISRM suggested method for the complete stress-strain curve for intact rock in uniaxial compression," *International Journal of Rock Mechanics and Mining Sciences & Geomechanics Abstracts*, vol. 36, no. 3, pp. 279–289, 1999.

[25] J. He, L. M. Dou, S. Y. Gong, J. Li, and Z. Q. Ma, "Rock burst assessment and prediction by dynamic and static stress analysis based on micro-seismic monitoring," *International Journal of Rock Mechanics and Mining Sciences*, vol. 93, pp. 46–53, 2017.

[26] A. Taheri and F. Tatsuoka, "Small- and large-strain behaviour of a cement-treated soil during various loading histories and testing conditions," *Acta Geotechnica*, vol. 10, no. 1, pp. 131–155, 2014.

[27] R. Ulusay and J. A. Hudson, *The complete ISRM suggested methods for rock characterization, testing and monitoring: 1974-2006*, International Society for Rock Mechanics: ISRM Turkish National Group, Ankara, Turkey, 2009.

[28] P. Małkowski, Ł. Ostrowski, and J. Brodny, "Analysis of Young's modulus for Carboniferous sedimentary rocks and its relationship with uniaxial compressive strength using different methods of modulus determination," *Journal of Sustainable Mining*, vol. 17, no. 3, pp. 145–157, 2018.

[29] D. Lei, P. Zhang, J. T. He, P. X. Bai, and F. P. Zhu, "Fatigue life prediction method of concrete based on energy dissipation," *Construction and Building Materials*, vol. 145, no. 2017, pp. 419–425, 2017.

[30] R. Tepfers, B. Hedberg, and G. Szczekocki, "Absorption of energy in fatigue loading of plain concrete," *Matériaux et Construction*, vol. 17, no. 1, pp. 59–64, 1984.

[31] R. Vidya Sagar, D. S. Mohit, S. Deepak, and P. R. Desai, "Statistical analysis of acoustic emissions generated during unconfined uniaxial compression of cementitious materials," *Construction and Building Materials*, vol. 225, no. 20, pp. 692–708, 2019.

[32] M. Naderloo, M. Moosavi, and M. Ahmadi, "Using acoustic emission technique to monitor damage progress around joints in brittle materials," *Theoretical and Applied Fracture Mechanics*, vol. 104, article 102368, 2019.

[33] X. Wang, Z. J. Wen, Y. J. Jiang, and H. Huang, "Experimental study on mechanical and acoustic emission characteristics of rock-like material under non-uniformly distributed loads," *Rock Mechanics and Rock Engineering*, vol. 51, no. 3, pp. 729–745, 2018.

[34] L. H. Tan, T. Ren, X. H. Yang, and X. Q. He, "A numerical simulation study on mechanical behaviour of coal with bedding planes under coupled static and dynamic load," *International Journal of Mining Science and Technology*, vol. 28, no. 5, pp. 791–797, 2018.

[35] P. Sedlak, Y. Hirose, S. A. Khan, M. Enoki, and J. Sikula, "New automatic localization technique of acoustic emission signals in thin metal plates," *Ultrasonics*, vol. 49, no. 2, pp. 254–262, 2009.

[36] K. Luxbacher, E. Westman, P. Swanson, and M. Karfakis, "Three-dimensional time-lapse velocity tomography of an underground longwall panel," *International Journal of Rock Mechanics and Mining Sciences*, vol. 45, no. 4, pp. 478–485, 2008.

[37] N. Hosseini, "Evaluation of the rockburst potential in longwall coal mining using passive seismic velocity tomography and image subtraction technique," *Journal of Seismology*, vol. 21, no. 5, pp. 1101–1110, 2017.